Renewable Energy 181 (2022) 535–553

Contents lists available at ScienceDirect

Renewable Energy

journal homepage: www.elsevier.com/locate/renene

Thermal modelling and experimental evaluation of a novel concentrating photovoltaic thermal collector (CPVT) with parabolic concentrator

Hossein Afzali Gorouh [a], Mazyar Salmanzadeh [a], Pouriya Nasseriyan [a], Abolfazl Hayati [b, *], Diogo Cabral [b], João Gomes [b, c], Björn Karlsson [b]

[a] Department of Mechanical Engineering, Shahid Bahonar University of Kerman, Kerman, 76169-14111, Iran
[b] Department of Building Engineering, Energy Systems and Sustainability Science, University of Gävle, Kungsbäcksvägen 47, 801 76, Gävle, Sweden
[c] R&D Department, MG Sustainable Engineering AB, Börjegatan 41B, 752 29, Uppsala, Sweden

ARTICLE INFO

Article history:
Received 25 April 2021
Received in revised form
5 August 2021
Accepted 9 September 2021
Available online 16 September 2021

Keywords:
Photovoltaic-thermal collector
Parabolic concentrator
Thermal modelling
Primary energy

ABSTRACT

In the present study, a zero-dimensional thermal model has been developed to analyze a novel low concentration photovoltaic-thermal (CPVT) collector. The model has been developed by driving heat transfer and energy balance equations for each part of the collector and then solving all the equations simultaneously. Moreover, a Monte-Carlo ray-tracing software has been used for optical stimulations of the parabolic trough solar collector. The novel CPVT collector has been experimentally tested at Gävle University (Sweden) and the model has been validated against the experimental results. The primary energy saving equivalent to the thermal-electrical power cogeneration of the CPVT collector has been determined. The effect of glass cover removal, heat transfer fluid (HTF) inlet temperature and mass flow rate on the collector performance has been investigated. The optimum HTF mass flow rates of the collector for maximum electrical yield and overall primary energy saving were determined under specified operating conditions by considering the pump consumption. The effect of mean fluid temperature on the thermal and electrical efficiencies has been studied and the characteristic equation of the thermal efficiency has been obtained. The thermal and electrical peak efficiencies of the collector have been found to be 69.6% and 6.1%, respectively.

1. Introduction

Solar Energy is a sustainable and emission-free source of energy, which can be used by photovoltaic (PV) cells to produce electricity. Conventional PV cells have electrical efficiencies with a range of 5–20% [1]. Therefore, more than 80% of solar energy is reflected towards the atmosphere or dissipated as heat, which raises the cell temperature. Moreover, as the PV cell temperature increases, the cell efficiency drops [2]. Therefore, it is a good idea to extract the dissipated thermal energy by a heat transfer fluid (HTF). So, the concept of photovoltaic-thermal (PVT) collectors can be introduced to generate thermal energy (heat) as well as electricity generation from the same gross area. Concentrating Photovoltaic (CPV) can be identified to replace relatively expensive PV cells with cheaper reflectors to lower the cost [3]. But the main concern that lies with CPV technologies is the high temperatures that the PV cell reaches due to concentration. Thus, a cooling fluid is essential to lower the cell temperature. Concentrating photovoltaic thermal (CPVT) collectors are a combination of PVT and CPV collectors that generate thermal and electrical energy simultaneously which also need less installation area in comparison with separate PV and thermal collectors.

Garg and Adhikari [4] developed a theoretical steady-state model for a PVT system combined with a compound parabolic concentrator (CPC). The results indicated that the PVT system with concentrator performs better than the PVT system without concentrator. The performance analysis of a parabolic trough concentrator (PTC) combined with a PVT system was carried out by Coventry [5] which showed a significant impact of non-uniform illumination on electrical yield of the collector. Also, a combined electrical and thermal efficiency of 69% was reported for the collector under typical operating conditions. Nilsson et al. [6]

* Corresponding author.
E-mail address: Abolfazl.Hayati@hig.se (A. Hayati).

https://doi.org/10.1016/j.renene.2021.09.042

Nomenclature

A_{bond}	Area of the bond between copper plates and copper tube [m^2]
A_g	Effective area of glass cover [m^2]
A_p	Copper plates Area [m^2]
A_{pv}	Effective area of PV cells [m^2]
A_r	Effective area of reflector (concentrator) [m^2]
A_t	Copper tube Area [m^2]
$C_{p,f}$	Specific heat capacity of HTF [J/kg.K]
D_t	Copper tube inner diameter [m]
$E_{p,t}$	Total primary energy saving [W]
$F_{g,pv}$	View factor of glass cover to PV cells
$F_{g,r}$	View factor of glass cover to reflector (concentrator)
f_l	Darcy friction factor of HTF flow inside the copper tube
$f_{p,e}$	Primary energy factor of electricity
$f_{p,h}$	Primary energy factor of heating (district)
$F_{pv,r}$	View factor of PV cells to reflector (concentrator)
g	Gravitational acceleration [m/s^2]
G_t	Global solar irradiation [W/m^2]
hc_b	Convective heat transfer coefficient between inner side of rear cover and reflector [$W/m^2.K$]
hc_g	Convective heat transfer coefficient between glass cover and inside air [$W/m^2.K$]
hc_p	Average convective heat transfer coefficient between the copper plates and inside air [$W/m^2.K$]
hc_{p1}	Convective heat transfer coefficient between the right copper plate and inside air [$W/m^2.K$]
hc_{p2}	Convective heat transfer coefficient between the left copper plate and inside air [$W/m^2.K$]
hc_{pv}	Average convective heat transfer coefficient between the PV modules and inside air [$W/m^2.K$]
hc_{pv1}	Convective heat transfer coefficient between the right PV module and inside air [$W/m^2.K$]
hc_{pv2}	Convective heat transfer coefficient between the left PV module and inside air [$W/m^2.K$]
hc_r	Convective heat transfer coefficient between reflector and inside air [$W/m^2.K$]
hc_{r1}	Convective heat transfer coefficient between r_1 (left equivalent plate of the reflector) and inside air [$W/m^2.K$]
hc_{r2}	Convective heat transfer coefficient between r_2 (middle equivalent plate of the reflector) and inside air [$W/m^2.K$]
hc_{r3}	Convective heat transfer coefficient between r_3 (right equivalent plate of the reflector) and inside air [$W/m^2.K$]
h_f	Convective heat transfer coefficient of HTF [$W/m^2.K$]
$hr_{g,amb}$	Radiative heat transfer between glass cover and ambient [$W/m^2.K$]
h_w	Convective heat transfer between glass cover and ambient [$W/m^2.K$]
J_g	Glass cover radiosity [W/m^2]
J_{pv}	PV cells radiosity [W/m^2]
J_r	Reflector (concentrator) radiosity [W/m^2]
$k_{b,air}$	Air thermal conductivity reflector at average temperature of rear cover and reflector [W/m.K]
k_{bond}	Thermal conductivity of the bond between copper plates and copper tube (soldering) [W/m.K]
k_{cu}	copper thermal conductivity [W/m.K]
k_f	Thermal conductivity of HTF (water) [W/m.K]
$k_{g,air}$	Air thermal conductivity at glass cover film temperature $(T_g+T_{air})/2$ [W/m.K]
$k_{p,air}$	Air thermal conductivity at copper plates film temperature $(T_p+T_{air})/2$ [W/m.K] [W/m.K]
k_{pv}	PV cells thermal conductivity [W/m.K]
$k_{pv,air}$	Air thermal conductivity at PV modules film temperature $(T_{pv}+T_{air})/2$ [W/m.K]
$k_{r,air}$	Air thermal conductivity at reflector film temperature $(T_r+T_{air})/2$ [W/m.K]
k_{si}	Silicone thermal conductivity [W/m.K]
L	Effective length of the collector [m]
L_t	Copper tube length [m]
$\dot{m}_f$	HTF mass flow rate [kg/s]
Nu_b	Nusselt number for inner side of rear cover
Nu_f	HTF Nusselt number
Nu_g	Nusselt number for glass cover inner side
Nu_{p1}	Nusselt number for the right copper plate
Nu_{p2}	Nusselt number for the left copper plate
Nu_{pv1}	Nusselt number for the right PV module
Nu_{pv2}	Nusselt number for the left PV module
Nu_{r1}	Nusselt number for r_1 (left equivalent plate of the reflector)
Nu_{r2}	Nusselt number for r_2 (middle equivalent plate of the reflector)
Nu_{r3}	Nusselt number for r_3 (right equivalent plate of the reflector)
$p_{e,net}$	Net electrical power output [W]
$p_{e,pump}$	Pump electrical power consumption [W]
$p_{e,pv}$	PV cells electrical power generation [W]
Pr_f	HTF Prandtl number
Pr_g	Air Prandtl number at glass cover film temperature $(T_g+T_{air})/2$
Pr_p	Air Prandtl number at copper plates film temperature $(T_p+T_{air})/2$
Pr_{pv}	Air Prandtl number at PV modules film temperature $(T_{pv}+T_{air})/2$
Pr_r	Air Prandtl number at reflector film temperature $(T_r+T_{air})/2$
$q_{a,g}$	Absorbed solar radiation by glass cover [W]
$q_{a,p}$	Absorbed solar radiation by copper plates [W]
$q_{a,r}$	Absorbed solar radiation by reflector [W]
$q_{a,t}$	Absorbed solar radiation by copper tube [W]
$q_{b,amb}$	Heat transfer from rear cover to ambient [W]
$qc_{g,air}$	Convective heat transfer from inside air to glass cover [W]
$qc_{p,air}$	Convective heat transfer from copper plates to inside air [W]
$qc_{pv,air}$	Heat transfer from PV cells to inside air [W]
$qc_{r,air}$	Convective heat transfer between inner side of reflector and inside air [W]
$qc_{r,b}$	Convective heat transfer between outer side of reflector and inner side of rear cover [W]
$q_{g,amb}$	Convective heat transfer from glass cover to ambient [W]
$q_{p,t}$	Heat transfer from copper plates to copper tube [W]
$q_{pv,p}$	Heat transfer from PV cells to copper plates [W]
qr_g	Radiative heat transfer from glass cover [W]
qr_{pv}	Radiative heat transfer from PV cells [W]
qr_r	Radiative heat transfer from reflector (concentrator) [W]
$qr_{r,b}$	Radiative heat transfer between outer side of reflector and inner side of rear cover [W]
q_u	Useful thermal energy (thermal power output) [W]

$R_{b,amb}$	Thermal resistance between rear cover and ambient [K/W]
$Rc_{g,air}$	Thermal resistance between glass cover and inside air [K/W]
$Rc_{p,air}$	Convective thermal resistance between copper plates and inside air [K/W]
$Rc_{pv,air}$	Thermal resistance between PV modules and inside air [K/W]
$Rc_{r,air}$	Thermal resistance between reflector and inside air [K/W]
$Rc_{r,b}$	Thermal resistance between reflector and rear cover [K/W]
Re_f	Reynolds number of the HTF flow
$R_{g,amb}$	Thermal resistance between glass cover and ambient [K/W]
r_i	Inner radius of copper tube [m]
r_o	Outer radius of copper tube [m]
$R_{p,t}$	Thermal resistance between copper plates and copper tube [K/W]
$R_{pv,p}$	Thermal resistance between PV modules and copper plates [K/W]
S_p	Concentrated solar irradiation on copper plates [W/m^2]
S_{pv}	Concentrated solar irradiation on the PV cells [W/m^2]
S_r	Incident solar irradiation on reflector [W/m^2]
S_t	Concentrated solar irradiation on copper tube [W/m^2]
T_{air}	Inside air mean temperature [K]
T_{amb}	Ambient temperature [K]
T_b	rear cover temperature [K]
T_g	Glass cover mean temperature [K]
th_{bond}	thickness of the bond between copper plates and copper tube [m]
th_p	copper plates thickness [m]
th_{pv}	PV cells thickness [m]
th_{si}	Silicone thickness [m]
$T_{i,f}$	HTF inlet temperature [K]
$T_{m,f}$	Mean HTF temperature [K]
$T_{o,f}$	HTF outlet temperature [K]
T_p	Copper plates mean temperature [K]
T_{pv}	PV cells mean temperature [K]
T_r	Reflector (concentrator) mean temperature [K]
T_{ref}	Reference temperature for standard test condition (= 25°C)
T_t	Copper tube mean temperature [K]
V_f	HTF velocity [m/s]
V_w	Wind speed [m/s]
$w_{b,e}$	Equivalent width between rear cover and reflector [m]
w_g	Glass cover width [m]
w_p	copper plates width [m]
w_{pv}	PV modules width [m]
w_{r1}	Width of r_1 (left equivalent plate of the reflector) [m]
w_{r2}	Width r_2 (middle equivalent plate of the reflector) [m]
w_{r3}	Width of r_3 (right equivalent plate of the reflector) [m]

Greek Symbols

α_b	Air thermal diffusivity at average temperature of rear cover and reflector [m^2/s]
α_g	Glass cover absorptivity
α_p	Copper plates absorptivity
α_r	Reflector absorptivity
α_t	Copper tube absorptivity
β_{air}	Volumetric thermal expansion of inside air at its average temperature T_{air} [K^{-1}]
β_b	Volumetric thermal expansion of inside air at average temperature of rear cover and reflector $(T_b+T_r)/2$ [K^{-1}]
β_{pv}	PV cells temperature coefficient
ΔP_l	Collector pressure drop [Pa]
ε_b	rear cover emissivity
ε_g	Glass cover emissivity
ε_{pv}	PV cells emissivity
ε_r	Reflector (concentrator) emissivity
$\varepsilon_{r,b}$	Emissivity of outer side of reflector
η_e	Collector electrical efficiency
$\eta_{e,m}$	PV module efficiency
η_{pump}	Pump efficiency
$\eta_{ref,m}$	PV module efficiency at standard test condition (Solar cell temperature of 25°C and Solar irradiation of 1000W/m^2 with solar spectrum air mass of 1.5)
η_{th}	Collector thermal efficiency
θ_g	Angle of glass cover inclination from gravity direction [°]
θ_{p1}	Angle of the right copper plate inclination from gravity direction [°]
θ_{p2}	Angle of the left copper plate inclination from gravity direction [°]
θ_{pv1}	Angle of the right PV module inclination from gravity direction [°]
θ_{pv2}	Angle of the left PV module inclination from gravity direction [°]
θ_{r1}	Angle of r_1 (left equivalent plate of the reflector) inclination from gravity direction [°]
θ_{r2}	Angle of r_2 (middle equivalent plate of the reflector) inclination from gravity direction [°]
θ_{r3}	Angle of r_3 (right equivalent plate of the reflector) inclination from gravity direction [°]
θ_t	Collector tilt angle [°]
ν_b	Air kinetic viscosity at average temperature of rear cover and reflector [m^2/s]
ν_g	Air kinetic viscosity at glass cover film temperature $(T_g+T_{air})/2$ [m^2/s]
ν_p	Air kinetic viscosity at copper plates film temperature $(T_p+T_{air})/2$ [m^2/s]
ν_{pv}	Air kinetic viscosity at PV modules film temperature $(T_{pv}+T_{air})/2$ [m^2/s]
ν_r	Air kinetic viscosity at reflector film temperature $(T_r+T_{air})/2$ [m^2/s]
ρ_f	HTF density [kg/m^3]
ρ_g	Glass cover reflectivity
ρ_r	Reflector (concentrator) reflectivity
σ	Stefan-Boltzmann constant [$=5.67\times10^8$ W/m^{2}K^4]
τ_g	Glass cover transmissivity

Abbreviations

CPC	Compound Parabolic Collectors
CPV	Concentrating Photovoltaic
CPVT	Concentrating Photovoltaic-Thermal
HTF	Heat transfer fluid
PV	Photovoltaic
PVT	Photovoltaic-Thermal

evaluated a PVT-CPC hybrid system for high latitudes. The yearly output power was discussed in different cases and the optimum characteristics of the system were determined. Bernardo et al. [7] introduced a testing and characterization method for performance evaluation of CPVT hybrid systems. A finite-volume model of a PVT collector integrated with a parabolic concentrator was developed by Calise et al. [8] for energy and exergy evaluation of the collector. From both energy and exergy perspectives, the system performance showed a significant sensitivity to the flow rate of the HTF.

Bahaidarah et al. [9] evaluated the thermal and electrical performances of a flat plate PV and a PV-CPC system numerically and experimentally. Also, they compared the performances of the two systems with and without cooling fluid. The generated electricity of the PV-CPC collector with cooling was about twice of the collector electricity generation with no cooling fluid. They deduced that the electrical yield of the PV-CPC is much more than the flat plate PV (39% vs 23%) in all cases. Atheaya et al. [10] developed a characteristic equation for a partially covered PVT-CPC collector by deriving energy balance equations of the collector components. Several cases with different configurations were studied and compared. Tripathi et al. [11] presented a thermal model for a combination of N series-connected partially covered PVT-CPC collectors. The thermal performance, overall exergy and the outlet HTF temperature of the collectors were studied in different cases. They found the combination of PVT-CPC collectors, which 25% partially covered by PV cells, is the best choice for maximum thermal energy. Also, the combination of fully covered (100% covered by cells) PVT-CPC collectors reported as the best case from the overall exergy point of view. Tiwari et al. [12] presented a modified Hottel-Whillier-Bliss (HWB) equation for a combination of PVT-CPC collectors.

Koronaki and Nitsas [13] performed a numerical and experimental analysis of five series-connected PVT-CPC collectors. It was understood that as the inlet temperature of the HTF increased, the heat losses increased and the thermal performance of the system decreased. Conversely, as the HTF mass flow rate increased, the thermal performance of the system was increased because of higher convective heat transfer to the HTF. The electrical and thermal performance of four symmetric CPVT collectors with a vertical bifacial receiver were evaluated for low latitudes by Cabral and Karlsson [14]. The evaluation of the collectors with different geometries performed by a ray-tracing software and a multi-paradigm numerical computation. The results indicated that the CPC-PVT geometries delivered higher electrical and thermal power over a year. Maatallah and Youssef [15] presented a coupled opto-thermal model for a CPVT collector with insulation on three sides of the rectangular receiver. The temperature distribution, thermal and electrical performances of the system were studied. It was concluded that assuming uniform concentrated solar radiation on the receiver led to thermal efficiency overestimation. Zhang et al. [16] compared electrical and thermal performances of a CPVT system with a flat plate PVT system experimentally and theoretically. It was found that the generated electrical and thermal powers of the CPVT system were about 3 and 2 times higher than the flat plate system, respectively. A numerical and experimental study on the Solarus CPVT collector was performed by Nasseriyan et al. [17]. Temperatures of various layers of the receiver were measured by several k-type thermocouples and compared to the numerical simulation results to experimentally validate the numerical simulation. The effect of several parameters such as collector tilt angle, HTF temperature and mass flow rate, backside insulation and removing glass cover on the collector performance were investigated by the stimulation. It was reported that generated electricity of the unglazed collector was increased by 2% but the thermal yield was decreased by 70%.

In the present study, a novel CPVT solar collector with a low concentration ratio was designed, built and tested at the University of Gävle. The novel CPVT collector consists of an A-Shape PVT receiver core and a glazed stationary parabolic concentrator which is a new prototype. A zero-dimensional (0-D) thermal model based on energy balance is developed to investigate the thermal and electrical performance of the proposed novel CPVT collector. The model can predict average temperatures of the collector's main components during a day. To the best of the authors' knowledge, this kind of modelling has not been performed in literature for this type of CPVT collector. Experimental tests are also performed to validate the developed model of the collector. After validating the model, a parametric study is done to find the key design parameters of the novel CPVT collector for further optimizations.

2. CPVT collector description (geometry)

Fig. 1 describes the fabricated collector prototype which is composed of three troughs, one CPV and two identical CPVT troughs, however, this study focuses on the CPVT troughs of the collector.

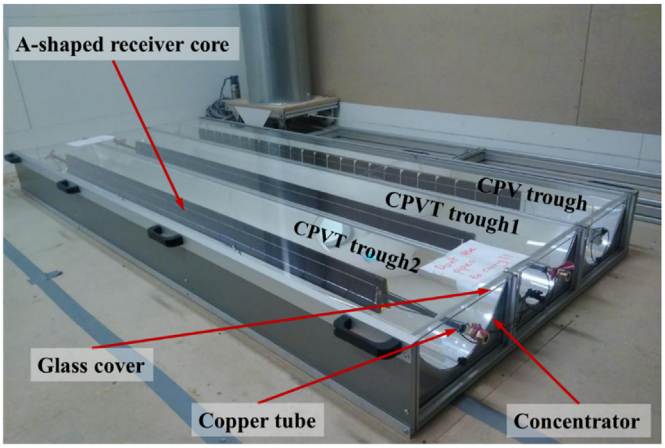

Fig. 1. Solar collector prototype at the University of Gävle.

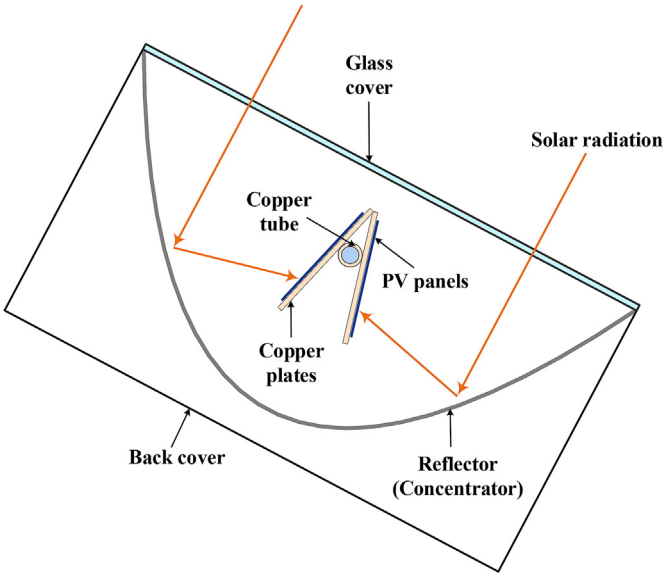

Fig. 2. Cross-section view of the CPVT troughs.

The cross-section view of a CPVT trough of the collector is shown in Fig. 2. The collector is sealed by a high transmittance low-iron solar glass and by transparent side gables. Therefore, the solar collector is considered airtight. Two small waterproof air vents are installed on both ends of the CPVT trough to remove the moisture of the inside air and protect the PV panels. The airflow from these air vents has been neglected. The reflective surface of the parabolic concentrator is made of high reflectance material which reflects the solar irradiance towards the receiver core.

As Fig. 2 indicates, the solar irradiation is reflected and concentrated on the receiver core by the reflector (concentrator). The receiver core of the collector is composed of two copper plates and a copper tube placed between the plates. The copper plates and copper tube are covered with black coating to absorb the maximum possible solar irradiation. The outer section of the copper plates is covered with monocrystalline PV cells. Each CPVT trough has two PV cell strings, each one with 24 quarter-sized PV cells connected in series. A portion of the concentrated solar flux received on the PV cells is converted to electricity and the remaining to heat. A portion of the generated heat is dissipated to the surroundings and the rest is transferred to the heat transfer fluid (HTF) as the useful thermal energy of the CPVT collector. To avoid the end shade effect, there is a 19 cm gap between the end of the concentrator and the receiver core. The CPVT collector design parameters are given in Table 1.

3. CPVT collector modelling

To investigate the thermal and electrical performance of the CPVT collector, a thermal model has been developed by driving energy balance and heat transfer equations for each part of the collector. Also, optical modelling is needed to determine the concentrated solar irradiation on the receiver core and use this value as an input for the thermal model.

3.1. Optical modelling

The concentrator curve is a pure parabola with a height of 13.9 cm and a focal length of 4.9 cm. The concentrator is made of high reflectance material with 92% reflectivity. The concentrator is covered by solar glass with a transmissivity of 91%. The two flat plates of the receiver core are identical with a dimension of 8 × 200 cm. The angle between the two flat plates is 20°.

Table 1
Design parameters of CPVT collector.

Parameters	Values and Units
A_b, A_{bond}, A_g	0.748 m^2, 0.02 m^2, 0.644 m^2
A_p, A_{pv}	0.32 m^2, 0.32 m^2
A_r, A_t	0.867 m^2, 0.09 m^2
L, L_t	2 m, 2.46 m
$w_{b,e}$, w_g	0.07 m, 0.322 m
w_p, w_{pv}	0.08 m, 0.08 m
w_{r1}, w_{r2}, w_{r3}	0.192 m, 0.064 m, 0.192 m
th_{bond}, th_{si}	0.001 m, 0.001 m
th_{pv}, th_p	0.0004 m, 0.001 m
r_o,r_i	0.006 m, 0.005 m
D_t	0.01 m
k_{pv}, k_{cu}	158 W/m.K, 395 W/m.K
k_{bond}, k_{si}	65 W/m.K, 0.2 W/m.K
$\eta_{ref,m}$	0.138
β_{pv}	0.004 1/K
V_w	2.7 m/s
α_g, α_p	0.02, 0.95
α_t, α_r	0.95, 0.08
ε_g, ε_{pv}, ε_r	0.84, 0.8, 0.08
$\varepsilon_{r,b}$, ε_b	0.79, 0.09
ρ_g,ρ_r	0.07,0.92
τ_g	0.91

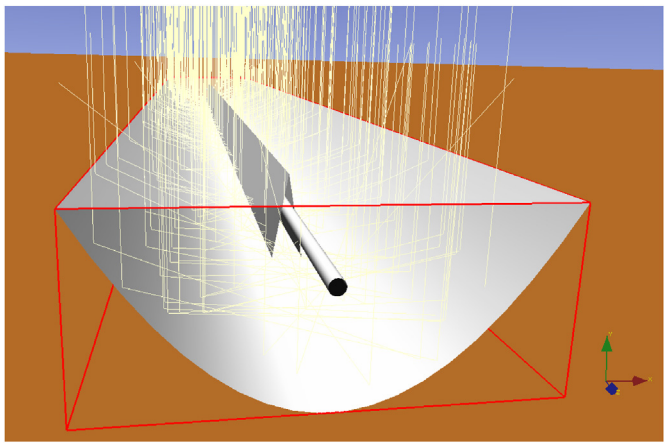

Fig. 3. 3-D view of the Optical Stimulation.

For optical analysis of the concentrating system, a Mont Carlo ray-tracing (MCRT) software named Tonatiuh was employed. Tonatiuh is open-source object-oriented software with a 3-D user-friendly interface developed for optical design and simulation of most concentrating solar systems. The ray-tracing software was experimentally validated for various concentrating solar systems [18,19].

The CPVT collector was modelled by defining various nodes and sub-nodes in the tree structure of the software. The reflectivity and transmissivity of the glass cover has been corrected for each incidence angle with the Fresnel equations. The reflector was considered free from fabrication errors. To achieve acceptable accuracy as well as lower computational time, the number of rays was set to 100,000 rays. The Sunlight (source of the rays) can be defined with sun position and shape. Sun position (azimuth and altitude angles) can be calculated by entering the date and the time into the software. Pillbox distribution was adequately considered for sun shape. In other words, the intensity distribution of sunlight over the solar disk has been assumed as uniform.

The optical stimulation was performed with an average concentrated solar flux on PV modules, copper plates, copper tube and concentrator were obtained from the stimulation and the values used as an input for the thermal modelling. Fig. 3 shows a 3-D view of the performed stimulation in the optical modelling software while the sun is normal to the collector's aperture.

3.2. Thermal modelling

To reduce the complexity of the theoretical thermal modelling, simplifications were assumed as follow:

1. The energy transfer was considered in quasi-steady condition.
2. The thicknesses of the glass cover, reflector and rear cover are small, therefore, have been neglected.
3. There is no-air leakage in the collector.
4. The air inside the collector is assumed as an ideal gas.
5. The water flow inside the copper tube is assumed fully developed through a smooth tube.
6. The radiation heat transfer between surfaces (glass cover, PV cells and reflector) was assumed as a radiation heat transfer with diffuse-gray surfaces. For the optical modelling, glass cover and reflector were assumed transparent and specular to the solar radiation, respectively.
7. The heat transfers from both side gables are small and therefore have been neglected.

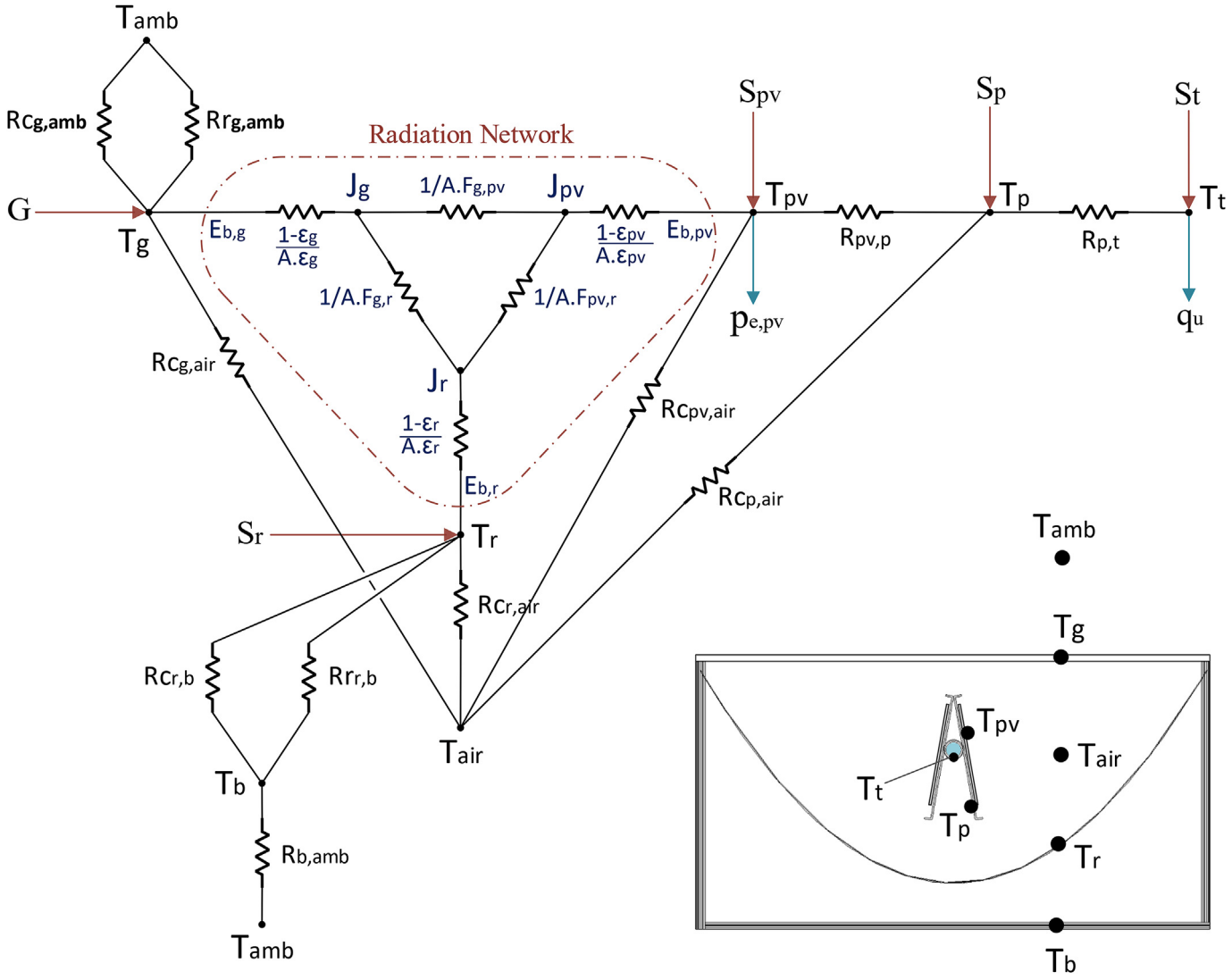

Fig. 4. Equivalent thermal resistance circuit of the CPVT.

8. For each component, a uniform mean bulk temperature was assumed.

The equivalent thermal resistance circuit of the thermal model is shown in Fig. 4. To solve this thermal circuit, all required heat transfer and energy balance equations were determined and derived for each node. All equations of the thermal model have entered in Engineering Equation Solver (EES) software and numerically solved simultaneously with built-in advanced iterative procedures. A relative residual tolerance of 1E-6 was considered as the stop criteria in the software.

The proposed heat transfer and energy balance equations for several nodes are presented and discussed in the following sections.

3.2.1. Radiative heat transfer between glass cover, reflector and PV cells (J_g, J_{pv} and J_r)

The radiative heat transfer between glass cover, reflector (concentrator) and PV cells was determined by the radiation network shown in Fig. 4. In the radiation network, the radiosity nodes (J_g, J_{pv} and J_r) are connected through relevant space resistance and the radiosity nodes are connected to the blackbody emissive powers associated with temperature nodes (T_g, T_{pv}, T_r) of each surface with relevant surface resistance [20].

The radiosities can be obtained by using a set of Eqs. (1)–(3). After determining the radiosities, the radiative heat transfer between these three surfaces can be determined by the other set of Eqs. (4)–(6). The view (configuration) factors were obtained by using the Hotel crossed string method [21]. The view factors of glass cover to PV cells ($F_{g,pv}$), glass cover to reflector ($F_{g,r}$) and PV cells to reflector ($F_{pv,r}$) were calculated to be 0.21, 0.79 and 0.6, respectively.

$$\frac{\sigma \cdot T_g{}^4 - J_g}{(1-\varepsilon_g)/(A_g \cdot \varepsilon_g)} = \frac{J_g - J_{pv}}{1/(A_g \cdot F_{g,pv})} + \frac{J_g - J_r}{1/(A_g \cdot F_{g,r})} \tag{1}$$

$$\frac{\sigma \cdot T_{pv}{}^4 - J_{pv}}{(1-\varepsilon_{pv})/(A_{pv} \cdot \varepsilon_{pv})} = \frac{J_{pv} - J_g}{1/(A_g \cdot F_{g,pv})} + \frac{J_{pv} - J_r}{1/(A_{pv} \cdot F_{pv,r})} \tag{2}$$

$$\frac{\sigma \cdot T_r{}^4 - J_r}{(1-\varepsilon_r)/(A_r \cdot \varepsilon_r)} = \frac{J_r - J_g}{1/(A_g \cdot F_{g,r})} + \frac{J_r - J_{pv}}{1/(A_{pv} \cdot F_{pv,r})} \tag{3}$$

$$qr_g = \left(\frac{\varepsilon_g \cdot A_g}{1-\varepsilon_g}\right) \cdot \left(\sigma \cdot {T_g}^4 - J_g\right) \tag{4}$$

$$qr_{pv} = \left(\frac{\varepsilon_{pv} \cdot A_{pv}}{1-\varepsilon_{pv}}\right) \cdot \left(\sigma \cdot {T_{pv}}^4 - J_{pv}\right) \tag{5}$$

$$qr_r = \left(\frac{\varepsilon_r \cdot A_r}{1-\varepsilon_r}\right) \cdot \left(\sigma \cdot {T_r}^4 - J_r\right) \tag{6}$$

3.2.2. Heat transfer and energy balance for glass cover

Heat is transferred from the outer side of the glass cover to the ambient by convection and radiation. The convective and radiative heat transfer coefficients are given by the following Eqs. (7) and (8) [22]:

$$h_w = 8.6 \cdot \frac{(V_w)^{0.6}}{L^{0.4}} \tag{7}$$

$$hr_{g,amb} = \varepsilon_g \cdot \sigma \cdot (T_g + T_{amb}) \cdot \left({T_g}^2 + {T_{amb}}^2\right) \tag{8}$$

Then the thermal resistance between glass cover and ambient can be obtained as follows (Eq. (9)):

$$R_{g,amb} = \frac{1}{A_g \cdot \left(h_w + hr_{g,amb}\right)} \tag{9}$$

$$hc_{pv1} = \frac{Nu_{pv1} \cdot k_{pv,air}}{w_{pv}} = \frac{0.54 \cdot \left(\frac{gr \cdot \beta_{air} \cdot (T_{pv} - T_{air}) \cdot {w_{pv}}^3}{{\nu_{pv}}^2} \cdot Pr_{pv} \cdot \mathrm{Cos}(\theta_{pv1})\right)^{0.25} \cdot k_{pv,air}}{w_{pv}} \tag{15}$$

$$hc_{pv2} = \frac{Nu_{pv2} \cdot k_{pv,air}}{w_{pv}} = \frac{0.54 \cdot \left(\frac{g \cdot \beta_{air} \cdot (T_{pv} - T_{air}) \cdot {w_{pv}}^3}{{\nu_{pv}}^2} \cdot Pr_{pv} \cdot \mathrm{Cos}(\theta_{pv2})\right)^{0.25} \cdot k_{pv,air}}{w_{pv}} \tag{16}$$

Also, heat is transferred from the inner side of glass cover to the air inside the collector by natural convection. The convective heat transfer coefficient and then the thermal resistance between the glass cover and inside air can be determined by the following Eqs. (10) and (11) [23]:

$$hc_g = \frac{Nu_g \cdot k_{g,air}}{w_g} = \frac{0.54 \cdot \left(\frac{g \cdot \beta_{air} \cdot (T_{air} - T_g) \cdot {w_g}^3}{{\nu_g}^2} \cdot Pr_g \cdot \mathrm{Cos}\theta_g\right)^{0.25} \cdot k_{g,air}}{w_g} \tag{10}$$

$$Rc_{g,air} = \frac{1}{A_g \cdot hc_g} \tag{11}$$

The energy balance for the glass cover can be derived as follows (Eq. (12)):

$$qr_g + qc_{g,air} + q_{a,g} = q_{g,amb} \tag{12}$$

Which can be rewritten as (Eq. (13)):

$$qr_g + \frac{(T_{air} - T_g)}{Rc_{g,air}} + \alpha_g \cdot G_t \cdot A_g = \frac{(T_g - T_{amb})}{R_{g,amb}} \tag{13}$$

3.2.3. Heat transfer and energy balance for PV cells

PV cells convert a portion of the concentrated solar irradiation to electricity depending on the cell efficiency, and the remaining converts to heat. As discussed previously, the efficiency of PV cells varies with temperature of the cells. To consider the temperature dependency of the PV modules standard efficiency, Eq. (14) is used [24]:

$$\eta_{e,m} = \eta_{ref,m} \cdot \left(1 - \beta_{pv} \cdot \left(T_{pv} - T_{ref}\right)\right) \tag{14}$$

where the temperature coefficient of PV cells (β_{pv}) and the PV modules standard efficiency ($\eta_{ref,m}$) are 0.004%/K and 13.8%, respectively.

A part of the generated heat is transferred to the inside air by convection and other surfaces by radiation. Most of the heat is transferred to the copper plates attached under the PV cells. The radiation part was determined and presented previously in section 3.2.1. The mean convective heat transfer coefficient from PV cells to the inside air can be obtained by an average between convective heat transfer coefficients from each PV panel (left and right) to the inside air by following Eqs. (15)–(17) [23]:

$$hc_{pv} = \frac{hc_{pv1} + hc_{pv2}}{2} \tag{17}$$

For PV modules encapsulation, two thin layers of silicone are placed on either side of the modules. Consequently, there are two conductive thermal resistances on both sides of the cells. The thermal resistances from PV cells to inside air and copper plate can be determined by Eqs. (18) and (19), respectively.

$$Rc_{pv,air} = \frac{1}{A_{pv} \cdot hc_{pv}} + \frac{th_{si}}{k_{si} \cdot (A_{pv}/2)} \tag{18}$$

$$R_{pv,p} = \frac{th_{si}}{k_{si} \cdot (A_{pv}/2)} + \frac{th_{pv}}{k_{pv} \cdot (A_{pv}/2)} \tag{19}$$

The energy balance for the PV modules can be derived as follows (Eq. (20)):

$$qr_{pv} + q_{pv,p} + qc_{pv,air} + p_{e,pv} = S_{pv} \cdot A_{pv} \tag{20}$$

Which can be restated as (Eq. (21)):

$$qr_{pv} + \frac{T_{pv} - T_p}{R_{pv,p}} + \frac{T_{pv} - T_{air}}{Rc_{pv,air}} + S_{pv} \cdot A_{pv} \cdot \eta_{e,m} = S_{pv} \cdot A_{pv} \tag{21}$$

3.2.4. Heat transfer and energy balance for the copper plates

A portion of the heat received on the copper plate is transferred to the inside air by natural convection (from the backside of the plates) and the rest is transferred to the copper tube attached between the copper plates by conduction. The copper tube is soldered to the copper plates and the heat is transferred to the tube through the bond.

Following Rich [25] and Churchill and Chu [26], the mean convective heat transfer coefficients for the copper plates can be obtained by the following Eqs. (22)–(24):

$$hc_{p1} = \frac{Nu_{p1} \cdot k_{p,air}}{w_p} = \frac{\left[0.68 + \left\{\frac{0.67 \cdot \left(g \cdot \beta_{air} \cdot \left(T_{pv} - T_{air}\right) \cdot {w_{pv}}^3 \cdot Pr_p \cdot \mathrm{Cos}\left(\theta_{p1}\right)/{\nu_{pv}}^2\right)^{1/4}}{\left(1 + \left(0.492/Pr_p\right)^{9/16}\right)^{4/9}}\right\}\right] \cdot k_{p,air}}{w_p} \tag{22}$$

$$hc_{p2} = \frac{Nu_{p2} \cdot k_{p,air}}{w_p} = \frac{\left[0.68 + \left\{\frac{0.67 \cdot \left(g \cdot \beta_{air} \cdot \left(T_{pv} - T_{air}\right) \cdot {w_{pv}}^3 \cdot Pr_p \cdot \mathrm{Cos}\left(\theta_{p2}\right)/{\nu_{pv}}^2\right)^{1/4}}{\left(1 + \left(0.492/Pr_p\right)^{9/16}\right)^{4/9}}\right\}\right] \cdot k_{p,air}}{w_p} \tag{23}$$

$$hc_p = \frac{hc_{p1} + hc_{p2}}{2} \tag{24}$$

The thermal resistances from copper plates to inside air and copper tube can be obtained as follows (Eqs. (25) and (26)):

$$Rc_{p,air} = \frac{1}{\left(A_p - A_{bond}\right) \cdot hc_p} \tag{25}$$

$$R_{p,t} = \frac{th_p}{k_{cu} \cdot \left(A_p/2\right)} + \frac{th_{bond}}{k_{bond} \cdot \left(A_{bond}/2\right)} + \frac{ln(r_o/r_i)}{2 \cdot \pi \cdot k_{cu} \cdot L} \tag{26}$$

Then the energy balance for the PV cells can be written as follows (Eq. (27)):

$$qc_{p,air} + q_{p,t} = q_{pv,p} + q_{a,p} \tag{27}$$

Which can be rewritten as (Eq. (28)):

$$\frac{T_p - T_{air}}{Rc_{p,air}} + \frac{T_p - T_t}{R_{p,t}} = \frac{T_{pv} - T_p}{R_{pv,p}} + \alpha_p \cdot S_p \cdot A_p \tag{28}$$

3.2.5. Useful thermal energy output and HTF outlet temperature

The received thermal energy to the copper tube is transferred to the HTF by forced convection. If the fluid flow regime is laminar ($Re_f < 2300$), the average Nusselt number (Nu_f) in constant heat flux and constant temperature conditions are equal to 4.36 and 3.66 [27], respectively. Otherwise, for transient and turbulent flow ($Re_f > 2300$), the convective heat transfer coefficient can be determined by Eq. (29) [28].

$$h_f = Nu_f \cdot k_f \Big/ D_t = \left(\frac{(f_l/8) \cdot \left(Re_f - 1000\right) \cdot Pr_f}{1 + \left(12.7 \cdot \left((f_l/8)^{1/2}\right) \cdot \left(\left(Pr_f{}^{2/3}\right) - 1\right)\right)}\right) \cdot \left(1 + (D_t/L_t)^{2/3}\right) \cdot k_f \Big/ D_t \tag{29}$$

Where:

$$f_l = \left(1.82 \cdot log\left(Re_f\right) - 1.64\right)^{-2} \tag{30}$$

The useful thermal energy and the HTF outlet temperature can be obtained from the following Eqs. (31) and (32):

$$q_u = h_f \cdot \pi \cdot D_t \cdot L \cdot \left(T_t - T_{m,f}\right) \tag{31}$$

$$T_{o,f} = T_{i,f} + \frac{q_u}{\dot{m}_f \cdot C_{p,f}} \tag{32}$$

As the HTF flows inside the copper pipe, it absorbs heat and its temperature rises. Constant heat flux or constant temperature assumptions can be considered for the copper tube to predict the HTF temperature distribution along the collector. The mean temperature can be determined by integrating the temperature distribution over the collector length. HTF mean temperature for constant heat flux and constant temperature conditions can be calculated by Eqs. (33) and (34), respectively.

$$T_{m,f} = \frac{T_{o,f} + T_{i,f}}{2} \tag{33}$$

$$T_{m,f} = T_t + \left(T_t - T_{i,f}\right) \cdot \left(\frac{\dot{m}_f \cdot C_{p,f}}{h_f \cdot \pi \cdot D_t \cdot L}\right) \cdot \left(\left(exp\left(-\frac{h_f \cdot \pi \cdot D_t \cdot L}{\dot{m}_f \cdot C_{p,f}}\right) - 1\right)\right) \quad (34)$$

In practice, the copper tube surface is neither in constant heat flux nor constant temperature conditions, but it's a combination of both. Performed calculations lead to almost the same overall results by both constant heat flux and temperature assumptions. Because of the asymmetry along the collector length and for simplicity, the constant heat flux was assumed in the present study.

3.2.6. Energy balance for copper tube

The energy balance equation for the copper tube is given by Eq. (35).

$$q_{p,t} + q_{a,t} = q_u \quad (35)$$

Which can be restated as (Eq. (36)):

$$\frac{T_p - T_t}{R_{p,t}} + \alpha_t \cdot S_t \cdot A_t = q_u \quad (36)$$

3.2.7. Heat transfer and energy balance for the reflector (concentrator)

Heat is transferred between the inner side of the reflector to the inside air by natural convection. To determine the free convective heat transfer coefficient between the reflector inner side and inside air and due to lack of empirical relations in literature for this specific geometry and condition, the reflector curve was simplified to three flat plates (r_1, r_2, r_3) with different inclinations as shown in Fig. 5.

The convective heat transfer coefficient for each equivalent plate can be calculated by Eqs. 37–39, and then mean convective heat transfer coefficient for the reflector can be determined by averaging (weighted) between the calculated coefficients as follows (Eq. (40)):

$$hc_{r1} = \frac{Nu_{r1} \cdot k_{r,air}}{w_{r1}} = \frac{0.54 \cdot \left[\left(\frac{g \cdot \beta_{air} \cdot (T_r - T_{air}) \cdot {w_{r1}}^3}{{\nu_r}^2}\right) \cdot Pr_r \cdot \mathrm{Cos}(\theta_{r1})\right]^{0.25} \cdot k_{r,air}}{w_{r1}} \quad (37)$$

$$hc_{r2} = \frac{Nu_{r2} \cdot k_{r,air}}{w_{r2}} = \frac{0.54 \cdot \left[\left(\frac{g \cdot \beta_{air} \cdot (T_r - T_{air}) \cdot {w_{r2}}^3}{{\nu_r}^2}\right) \cdot Pr_r \cdot \mathrm{Cos}(\theta_{r2})\right]^{0.25} \cdot k_{r,air}}{w_{r2}} \quad (38)$$

$$hc_{r3} = \frac{Nu_{r3} \cdot k_{r,air}}{w_{r3}} = \frac{0.54 \cdot \left[\left(\frac{g \cdot \beta_{air} \cdot (T_r - T_{air}) \cdot {w_{r3}}^3}{{\nu_r}^2}\right) \cdot Pr_r \cdot \mathrm{Cos}(\theta_{r3})\right]^{0.25} \cdot k_{r,air}}{w_{r3}} \quad (39)$$

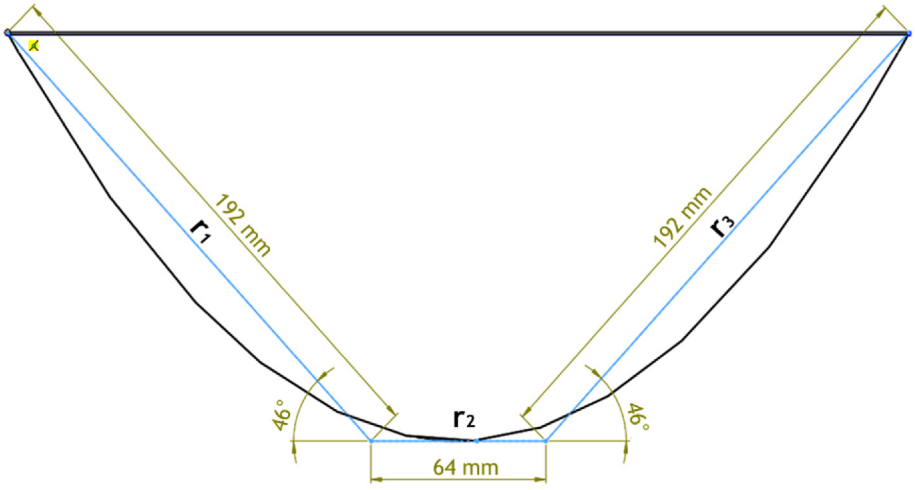

Fig. 5. Flat plates assumed as the reflector curve.

$$hc_r = \frac{hc_{r1} \cdot w_{r1} + hc_{r2} \cdot w_{r2} + hc_{r3} \cdot w_{r3}}{w_{r1} + w_{r2} + w_{r3}} \quad (40)$$

The mean convective thermal resistance between the inner side of reflector and inside air can be determined as (Eq. (41)):

$$Rc_{r,air} = \frac{1}{A_r \cdot hc_r} \quad (41)$$

Also, the heat is transferred from the outer side of the reflector to the inner side of the rear cover of the collector by convection and radiation. Due to the lack of relations for calculating the convective heat transfer coefficient, the heat transfer between the reflector and the rear cover has been assumed as a heat transfer between two flat plates with equivalent dimensions. The convective heat transfer coefficient and thermal resistance can be determined by the following correlations, respectively [29]:

$$hc_b = \frac{Nu_b \cdot k_{b,air}}{w} = \left[\left(\left\{1 + \left[0.212 \cdot \left(\frac{{w_{b,e}}^3 \cdot \beta_b \cdot g \cdot (T_r - T_b)}{\nu_b \cdot \alpha_b}\right)^{0.136}\right]^{11}\right\}^{1/11}\right) + \ldots$$
$$\ldots + \left(\frac{\theta_t}{60}\right) \cdot \left(\left[\left\{1 + \left[0.0566 \cdot \left(\frac{{w_{b,e}}^3 \cdot \beta_b \cdot g \cdot (T_r - T_b)}{\nu_b \cdot \alpha_b}\right)^{0.332}\right]^{4.76}\right\}^{1/4.76}\right]$$
$$- \left[\left\{1 + \left[0.212 \cdot \left(\frac{{w_{b,e}}^3 \cdot \beta_b \cdot g \cdot (T_r - T_b)}{\nu_b \cdot \alpha_b}\right)^{0.136}\right]^{11}\right\}^{1/11}\right]\right) \cdot \frac{k_{b,air}}{w_{b,e}} \quad (42)$$

$$Rc_{r,b} = \frac{1}{A_b \cdot hc_b} \quad (43)$$

As the outer side of the reflector can only see the rear cover, the view factor between the outer side of reflector and rear cover equals one. So, with reasonable accuracy, the radiation heat transfer between the surfaces can be considered as radiative heat transfer between two flat plates. The radiative heat transfer can be obtained from Eq. (44) [20].

$$qr_{r,b} = \frac{A_r \cdot \sigma \cdot \left(\left({T_r}^4\right) - \left({T_b}^4\right)\right)}{(1/\varepsilon_{r,b}) + (1/\varepsilon_b) - 1} \quad (44)$$

Then, the energy balance for the reflector can be obtained as (Eq. (45)):

$$qr_r + qc_{r,air} + qc_{r,b} + qr_{r,b} = q_{a,r} \quad (45)$$

Which can be rewritten as (Eq. (46)):

$$qr_r + \frac{T_r - T_{air}}{Rc_{r,air}} + \frac{T_r - T_b}{Rc_{r,b}} + qr_{r,b} = \alpha_r \cdot S_r \cdot A_r \quad (46)$$

3.2.8. Energy balance for inside air

The energy balance equation for the air inside the collector cavity can be written as (Eq. (47)):

$$qc_{g,air} + qc_{pv,air} + qc_{p,air} + qc_{r,air} = 0 \quad (47)$$

3.2.9. Heat transfer and energy balance for the rear cover

The heat transfer between the inner side of the rear cover and the outer side of reflector was determined earlier in section 3.2.7. To determine the heat transfer from the outer side of the rear cover to ambient, wind convective heat transfer is considered similar to the convective heat transfer calculation of the glass cover to ambient (section 3.2.2). Then the thermal resistance between the rear cover and ambient can be determined as follows (Eq. (48)):

$$R_{b,amb} = \frac{1}{h_w \cdot A_b} \quad (48)$$

The energy balance equation of the collector rear cover can be developed as (Eq. (49)):

$$qc_{r,b} + qr_{r,b} = q_{b,amb} \quad (49)$$

Which can be rewritten as (Eq. (50)):

$$\frac{T_r - T_b}{Rc_{r,b}} + qr_{r,b} = \frac{T_b - T_{amb}}{R_{b,amb}} \quad (50)$$

Finally, all the modified correlations in sections 3.2.1-3.2.9 will be added to an equation solver software and solved together simultaneously by iterative methods.

3.3. Energy analysis

As the CPVT collector is designed for a forced circulation, a pump is required HTF flow circulation through the collector loop. As the HTF flows through the collector loop, a pressure drop occurs and the circulation pump has to compensate the fluid pressure drop. In the present study, only the pressure drop due to the friction loss of the copper tube (collector pressure loss) was considered. Then the pump electricity consumption for HTF circulation along the collector can be calculated by the following Eq. (51) [30]:

$$p_{e,pump} = \frac{\left(\dot{m}_f \Big/ \rho_f\right) \cdot \Delta P_l}{\eta_{pump}} = \frac{\dot{m}_f \cdot f_l \cdot {V_f}^2 \cdot L_t}{2 \cdot \eta_{pump} \cdot D_t} \quad (51)$$

Where a constant value of 0.7 is considered for pump efficiency (η_{pump}). For fully developed laminar flow ($Re_f < 2300$), the friction

loss factor (f_l) can be determined by $64/Re_f$, otherwise, the friction factor can be obtained from Eq. (30).

The CPVT collector has electricity generation by PV cells and electricity consumption by the circulator pump. So, the net electrical power output can be determined by subtracting the consumption from the generation as follows (Eq. (52)):

$$p_{e,net} = p_{e,pv} - p_{e,pump} \tag{52}$$

Primary energy is the energy that has not been subjected to any conversion or transformation process [31]. The energy performance of the hybrid CPVT collector is presented as the primary energy equivalent of its thermal-electrical power generation to study the changes of both thermal and electrical production simultaneously in one concept. According to ISO 52000–1 [32], the primary energy factors for electricity ($f_{p,e}$) and heating ($f_{p,h}$) are 2.5 and 1.3, respectively. The total primary energy saving of the collector can be determined by Eq. (53).

$$E_{p,t} = f_{p,e} \cdot p_{e,net} + f_{p,h} \cdot q_u \tag{53}$$

4. Experimental setup

The novel solar collector was mounted in the HiG solar laboratory at Gävle University (latitude: 60°N, longitude: 17°E) for experimental analysis. The installed collector on the outdoor test stand of the laboratory is shown in Fig. 6.

Gävle University PVT test rig is indicated in Fig. 7. The indoor test setup consists of a hydraulic and electric loop to evaluate both thermal and electrical performance of solar PVT collectors.

The HTF (water) inlet temperature and mass flow rate can be defined by the user and the outlet temperature is measured to calculate the thermal power output of the collector. The water leaving the collector is cooled by a heat exchanger and stored in a tank. Then, the water is heated to the setpoint temperature of the inlet HTF by an electrical heater. This procedure is done to achieve a more stable inlet temperature into the collector which simplifies the measurement procedure.

An I–V tracer is used to plot the I–V curve and determine the electrical power output of the collector. The PV modules were tested in open circuit mode.

The ambient temperature and HTF inlet and outlet temperatures are measured by PT100 sensors with protective steel tubes. The HTF flow rate is measured by an electromagnetic flowmeter. The global and diffuse solar radiations are measured by Kipp&Zonen CMP3 and CMP6 Pyranometers. All regulations and controls are performed with an Abelko Webmaster PLC system and all the measured data are recorded every 30s by a Campbell Scientific CR1000 data logger. Although the data were collected at intervals of the 30s, hourly average data were calculated and presented in this study.

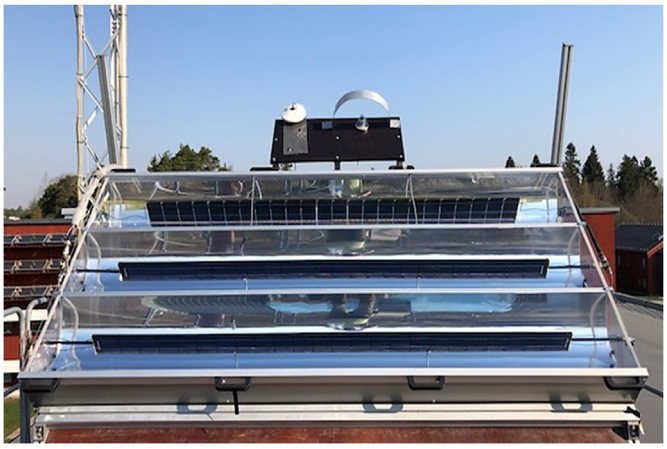

Fig. 6. Experimented solar collector at the outdoor test stand of HiG laboratory.

Fig. 7. HiG PVT indoor test setup at Gävle University.

To increase the measurement accuracy, a vacuum degasser is installed in the hydraulic loop to remove the dissolved air from the water. All pipes of the test rig are stainless steel pipes with insulation to prevent heat losses from pipes and obtain more accurate results.

The global solar radiation, ambient temperature, HTF flow rate, electrical power output, HTF inlet and outlet temperature of the south-facing stationary collector were measured for several summer days with various operating conditions. The experimental results of two days (July 27 and August 27) with perfect weather condition were selected based on ISO 9806:2013 SST testing method [33].

To analyze the collector performance at different operating conditions, the HTF inlet temperature and flow rate during July 27 were set to 20 °C and 0.5 l/m higher than August 27, respectively. The HTF inlet temperature and flow rate were kept almost constant during each day. To achieve the best optical performance, the collector tilt angle (θ_t) was set to 42° on July 27 and 52° on August 27 due to the lower solar altitude of August 27. For the daily measurements the collector is fixed throughout the days.

5. Result and discussion

In this part, first the experimental measurements during July 27 and August 27 are presented. The measured hourly solar radiation, the time and the date are used as inputs for the optical modelling software to determine the solar angles. Once the optical simulations were done for each hour (9:00 to15:00), the concentrated solar radiations on surfaces are determined from the simulation. The concentrated solar radiation, ambient temperature, HTF inlet temperature and flow rate were applied to the thermal model to calculate the heat and electricity generation of the collector. The developed model is validated by the experimental data for July 27 and August 27. Then, the effect of various operating conditions on the collector thermal and electrical output was investigated.

5.1. Experimental results

The experimental measurements on July 27 and August 27 are presented in Table 2 and Table 3, respectively. The results, including

Table 2
Experimental measurements on July 27.

Time (h)	Global solar radiation flux (W/m^2)	Ambient temperature (°C)	Inlet HTF temperature (°C)	Outlet HTF temperature (°C)	HTF flow rate (l/m)	Generated electricity per unit area of glass cover (W/m^2)
9:00	598	22.2	49.7	50.4	2.99	28.7
10:00	771	23.7	52.2	53.5	2.96	42.0
11:00	897	24.4	53.6	55.2	2.97	48.7
12:00	967	24.9	54.6	56.4	2.94	51.7
13:00	967	24.6	54.6	56.4	3.02	52.1
14:00	905	25.3	55.1	56.7	3.05	46.2
15:00	788	25.6	54.5	55.7	3.02	38.8

Table 3
Experimental measurements on August 27.

Time (h)	Global solar radiation flux (W/m^2)	Ambient temperature (°C)	Inlet HTF temperature (°C)	Outlet HTF temperature (°C)	HTF flow rate (l/m)	Generated electricity per unit area of glass cover (W/m^2)
9:00	551	19.6	29.2	30.3	2.51	27.7
10:00	722	22.5	29.5	31.1	2.50	41.3
11:00	868	24.4	29.6	31.6	2.49	50.2
12:00	935	25.6	29.6	31.8	2.49	53.5
13:00	935	26.5	29.5	31.7	2.49	52.2
14:00	862	27.2	29.4	31.6	2.49	46.6
15:00	685	27.4	29.4	31.2	2.45	40.2

global solar radiation flux, ambient temperature, HTF flow rate and its inlet and outlet as well as he produced electricity, are averaged for each hour from 8:30 to 15:30 and the midpoint of each time interval represents that hour interval (9:00–15:00).

5.2. Validation of the developed model

The thermal model validation is done by using the measured data with different solar radiation patterns, solar incident angles, ambient temperatures, HTF inlet temperatures and flow rates. The thermal and electrical power outputs based on effective glass area (A_g) are considered as validity variables. Fig. 8 and Fig. 9 present the comparison of experimental measurements and the modelling results per effective glass unit area for July 27 and August 27, respectively.

The graphs show that there is good agreement between the developed model and experimental results with average and maximum deviations of 6.5% and 12.4%, respectively, which is acceptable by considering the experimental measurement errors and the simplifying assumptions of the numerical model. Also, the experimental and numerical trends are almost the same and follow the solar radiation flux. So, it is concluded that the model gives realistic results and can be used for further analyses.

By comparing the measured solar radiation (Table 3) and the thermal power output (Fig. 9) at 13:00 and 14:00 of August 27, it is observed that the measured thermal power does not follow the solar radiation trend due to some measurement errors at these hours.

5.3. Mean temperature of the collector components

Mean temperature of different components such as PV cells (T_{pv}), copper plates (T_p), HTF ($T_{m,f}$), reflector (T_r), glass cover (T_g), inside air (T_{air}) are calculated by the proposed thermal model. The variation of the calculated mean temperatures and ambient

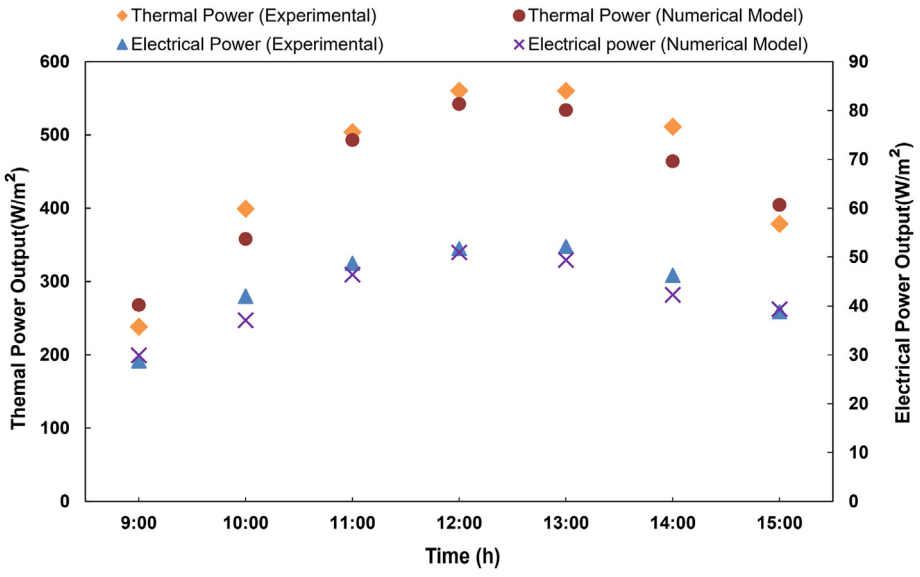

Fig. 8. Comparison of numerical and experimental results of July 27 (based on glass unit area).

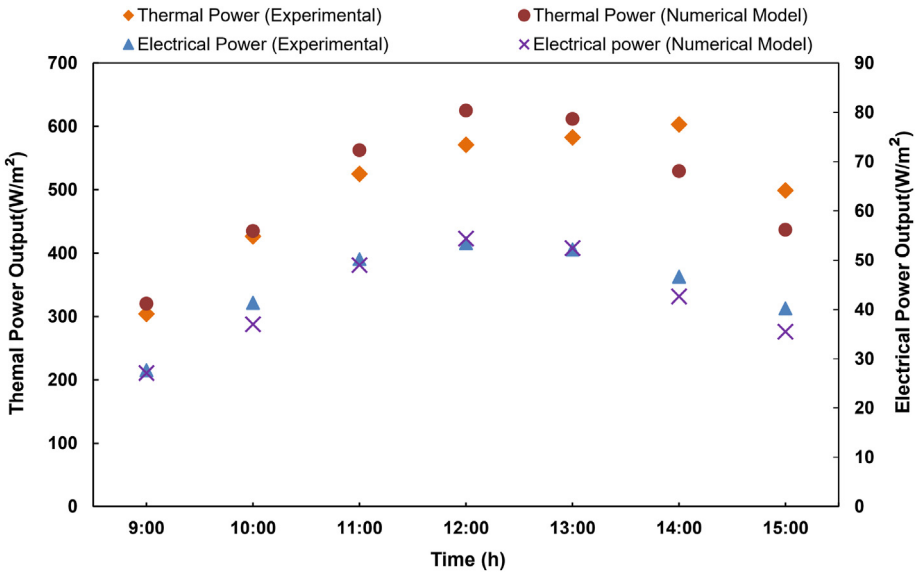

Fig. 9. Comparison of numerical and experimental results of August 27 (based on glass unit area).

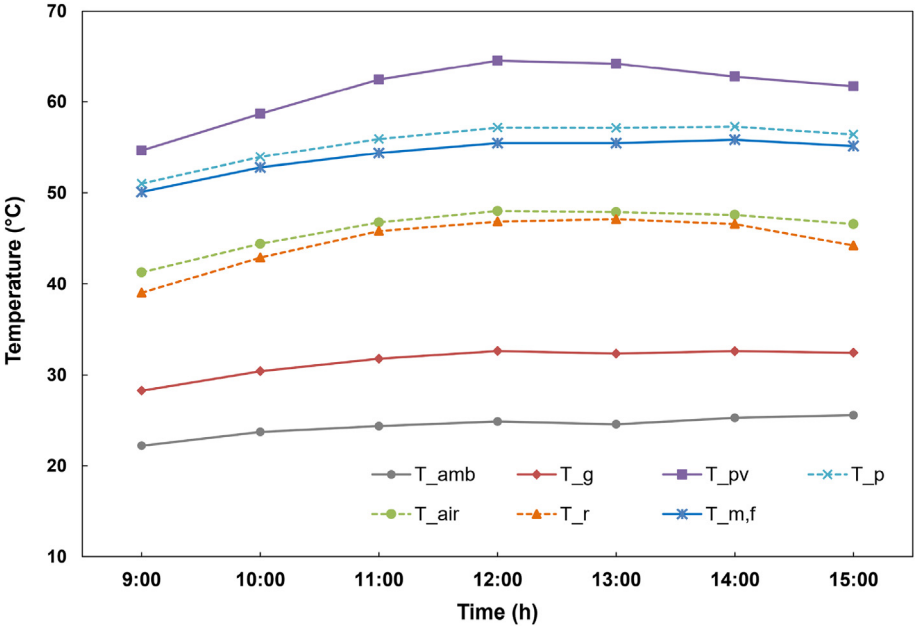

Fig. 10. Calculated mean temperature of various elements and ambient temperature during July 27.

temperature (T_{amb}) during July 27 and August 27 are presented in Fig. 10 and Fig. 11, respectively.

It is observed that for both days, the mean temperatures of components are mainly affected by three parameters: solar radiation, mean HTF temperature and ambient temperature. But for various components, the impact of each parameter is different due to thermal resistances and incident solar radiation. The trend of PV modules' mean temperature changes is closer to the solar radiation variations over the days due to the high incident solar radiation on the PV cells. The mean temperature of HTF and copper plates are close to each other and variation trends are almost the same due to the low thermal resistance between them. Also, the trend of the glass cover mean temperature is the same as ambient temperature because of low thermal resistance.

As demonstrated in Figs. 10 and 11, during both days, the maximum and minimum temperatures are observed in the PV cells and glass cover, respectively. Only at 14:00 and 15:00 of August 27, the reflector temperature is higher than the temperature of the cells because the sun rays miss the PV modules' surface, thus a higher absorbed solar radiation on the reflector than on the PV modules. The mean temperature of copper plates is higher than the temperatures of the reflector and inside air during July 27, while for August 27, it is the same only at 9:00 and the mean temperature of copper plates is lower than the temperatures of reflector and inside air from 11:00 onwards due to the lower mean HTF temperature of August 27.

5.4. Effect of glass cover removal

In this section, the effect of removing glass cover is investigated by the developed model. Consequently, the glass cover was removed in the optical and the thermal model and the results were calculated. For August 27, the thermal and electrical power outputs

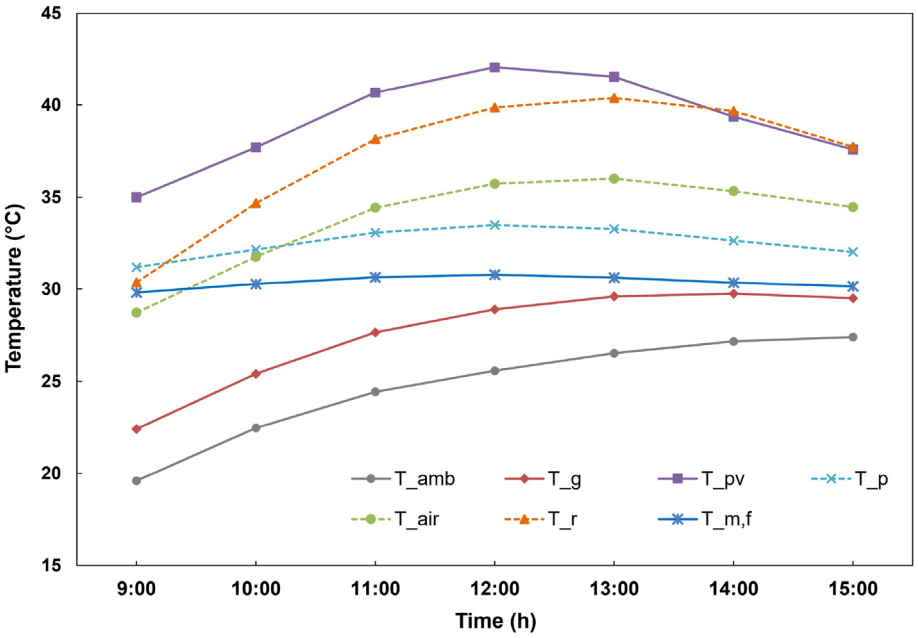

Fig. 11. Calculated mean temperature of various elements and ambient temperature during August 27.

of glazed and unglazed collectors per glass unit area of the CPVT collector are compared in Fig. 12.

It is understood that by removing the glass cover during August 27 (from 9:00 to 15:00), the optical losses will reduce (from optical simulation results) and the thermal power output will decrease by a daily average of 13% due to the increase of thermal losses while the electrical power will increase by a daily average of 10% due to PV cells temperature drop and optical losses reduction. Because the changes in thermal and electrical production by removing the glass cover are the opposite, the equivalent primary energy per glass unit area of the collector was determined and presented in Fig. 13.

It is observed that the electrical power increase (with relevant primary energy factor) could not compensate by the thermal power reduction (with relevant primary energy factor) and so the primary energy is decreased by removing the glass cover. As shown in Fig. 13, the percentage of the primary energy reduction by glass cover removal is reduced from 20% to 4% during the day (9:00–15:00) because of the thermal losses drop as a result of an increase in ambient temperature during the day. Also, due to the higher HTF inlet temperature on July 27 compared to August 27, it can be deduced that primary energy reduction is higher for July 27. So, the glazed collector has better overall energy performance and thermal yield, but the collector without glass cover is better for electricity yield.

5.5. Effect of HTF inlet temperature

To study the effect of HTF inlet temperature on the collector thermal and electrical power outputs, the HTF inlet temperature at noon on 27 August ($G_t = 935 W/m^2$) has been changed from 15 °C to

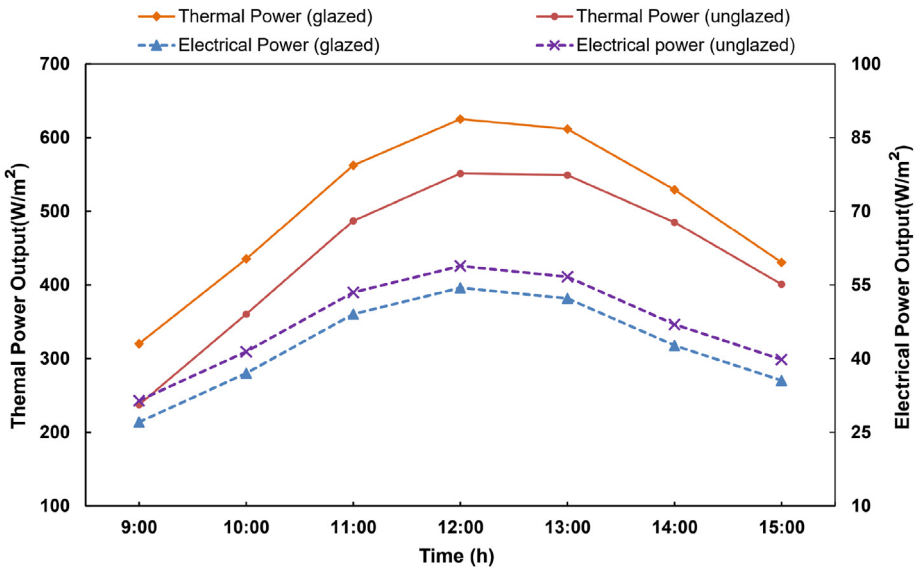

Fig. 12. Thermal and electrical power outputs per glass unit area of glazed and unglazed CPVT collector (August 27).

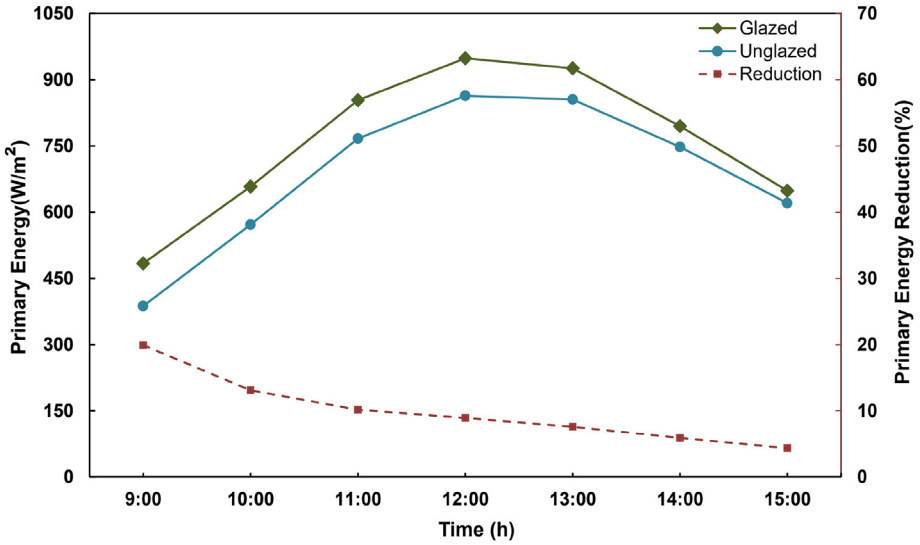

Fig. 13. Comparison of primary energy saving ($f_{p,e} = 2.5$, $f_{p,h} = 1.3$) by glazed and unglazed CPVT collector and the reduction in primary energy by removing glass cover (August 27).

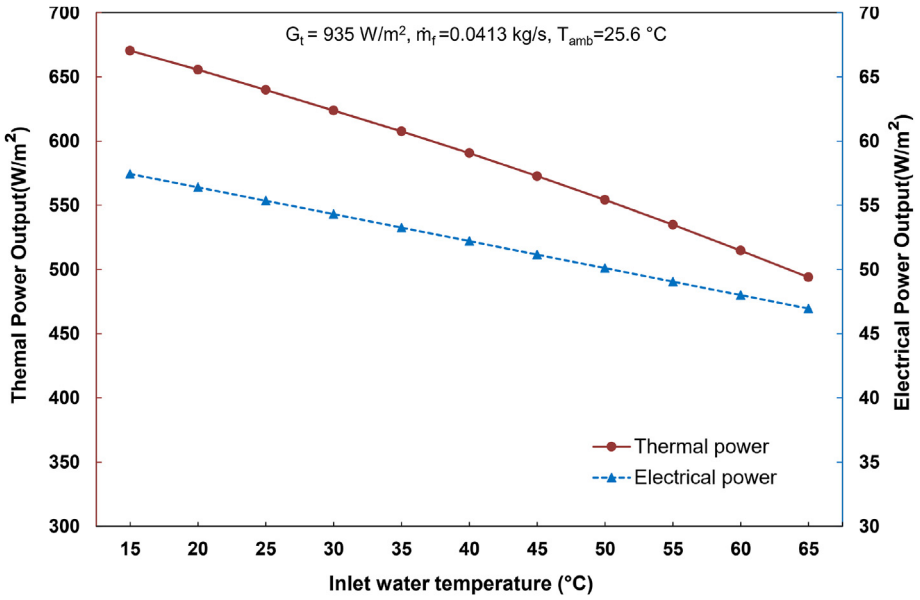

Fig. 14. Variation of the generated thermal and electrical power with the HTF (water) inlet temperature.

65 °C while other thermal model inputs such as solar radiation, ambient temperature and HTF flow rate were kept constant, then the thermal and electrical productions of the collector were calculated by the model. Fig. 14 shows the effect of HTF inlet temperature variation on the thermal and electrical yields per effective glass unit area of the CPVT collector.

It is found that by increasing the HTF inlet temperature, the thermal power decreases due to more heat losses and also the electrical power decreases because of higher PV cells temperature. Although the thermal power of the collector decreases by increasing the HTF inlet temperature, the HTF outlet temperature increases. So, the lower inlet temperature is better for the collector performance from the energy perspective (amount of energy) but it is not desirable from exergy perspective (quality of energy) and low-temperature heat is not suitable for direct use in a solar heating system. It is observed that by an increase of 50 °C in the HTF inlet temperature, the thermal and electrical power outputs decrease by 26% (177 W/m^2) and 18% (11 W/m^2), respectively. Thus, it can be understood that the thermal power output is more sensitive to the HTF inlet temperature.

5.6. Effect of HTF flow rate

In this section, the effect of the HTF flow rate on the collector power output is studied at noon on August 27 ($G_t = 935 W/m^2$). To attain this objective, the HTF mass flow rate was changed from 0.005 to 0.105 kg/s while other inputs were kept constant and the thermal power output, HTF outlet temperature, pump electricity consumption, PV cells electricity generation and the collector net electricity production were calculated from the developed model.

Variations of thermal power output per glass unit area and HTF outlet temperature with HTF mass flow rate are shown in Fig. 15. It is found that by increasing the HTF mass flow rate, the thermal power output increases due to the higher heat transfer rate from

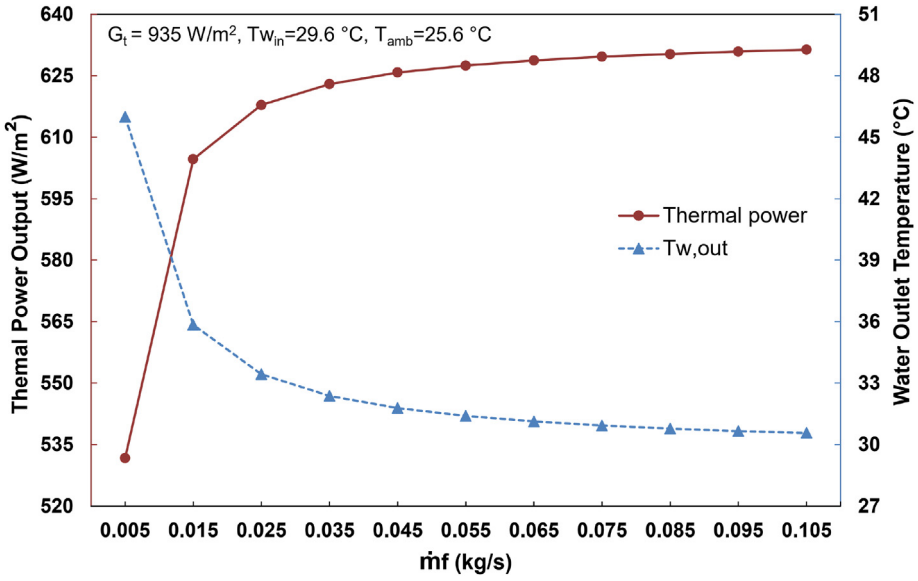

Fig. 15. Variation of thermal power and HTF (water) outlet temperature of the collector with HTF mass flow rate.

copper tube to HTF (higher h_f) and the HTF outlet temperature decreases because of more HTF mass flow rate that absorbs the heat. The variation trends are almost the same as typical heat exchangers with one side of constant heat flux. It is found that increasing HTF mass flow rate leads to a higher thermal power output with lower temperature and quality of energy.

Variation of the collector electricity generation, pump electricity consumption and the net electricity output per glass unit area with HTF mass flow rate are indicated in Fig. 16. It is understood that the electricity generation of the cells increases by increasing the mass flow rate because of the better heat removal of the cells and lower cell temperature. By increasing the HTF mass flow rate, the pump power consumption increases due to a higher pressure drop in the collector.

As indicated in Figs. 15 and 16, the rate of changes of thermal power output, HTF outlet temperature and electricity generation of PV cells are rapid in lower mass flow rate and then the rate of changes gradually decreases in higher mass flow rates due to the transition of laminar to turbulent flow. As the HTF mass flow rate increase from 0.005 to 0.015 kg/s, the Reynolds number increases from 936 to 2535 and the eddy motions start to appear in the flow (transient flow). Consequently, the heat transfer rate (Nusselt number) increases drastically and it can justify the significant changes in thermal power output, HTF outlet temperature and electricity generation. Therefore, the HTF mass flow rate shall be higher than 0.015 kg/s to attain better performance.

From Fig. 16, it can be observed that the net electricity generation of the collector will increase by increasing the mass flow rate to 0.045 kg/s and then decreases in higher flow rates because of a higher increase of pump consumption than the increase of cells electricity generation. So, the optimum mass flow rate for the net electricity generation of the collector is found to be 0.045 kg/s. For mass flow rates above 0.045 kg/s, although the net electricity generation decreases by increasing the HTF mass flow rate (Fig. 16),

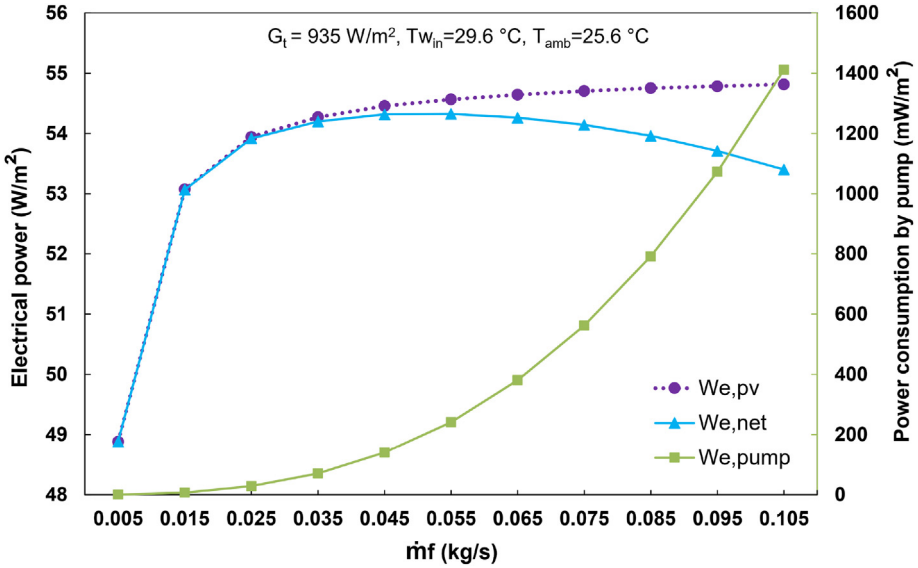

Fig. 16. Variation of PV cells electricity generation, pump electricity consumption and the collector net electricity output with HTF (water) mass flow rate.

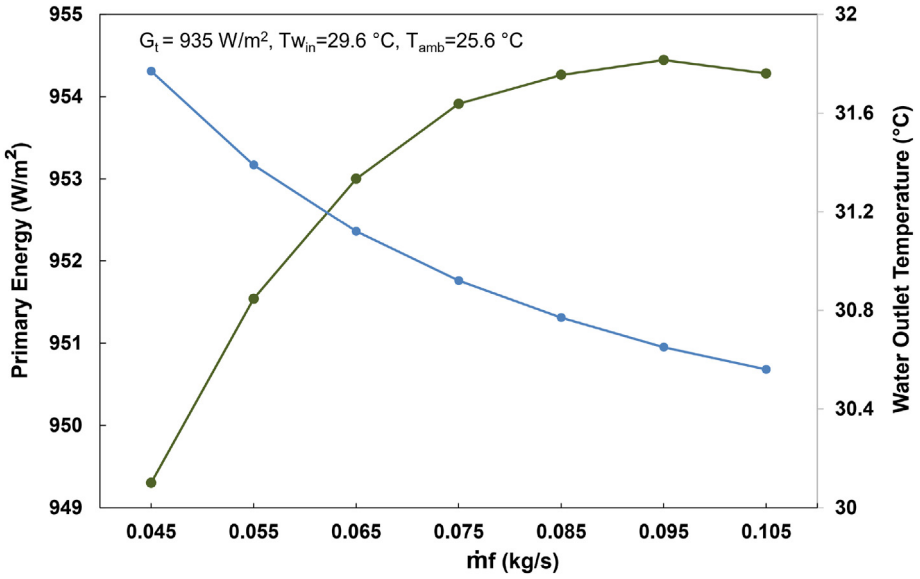

Fig. 17. Variation of the primary energy saving ($f_{p,e}$ = 2.5, $f_{p,h}$ = 1.3) and HTF (water) outlet temperature with HTF mass flow rate.

the thermal power generation increases (Fig. 15). So, the equivalent primary energy is calculated for different flow rates from 0.045 to 0.105 kg/s and the results are presented in Fig. 17. The optimum HTF mass flow rate with maximum primary energy saving is found to be 0.095 kg/s for the specific operating conditions. But the HTF outlet temperature (quality of the energy) must also be taken into account to be in a desirable range for the solar system.

5.7. Temperature dependence of thermal and electrical efficiencies

Thermal and electrical efficiencies of the CPVT collector based on effective glass unit area were determined for various temperature differences between fluid mean temperature and ambient temperature ($T_{m,f}$-T_{amb}) at noon on August 27 (G_t = 935W/m^2). To achieve this, the T_{amb} was kept constant at 20 °C and $T_{m,f}$ is changed from 25 °C to 75 °C. Then, the thermal and electrical efficiencies were calculated for temperature difference ($T_{m,f}$-T_{amb}) from 5 °C to 55 °C. It should be noted that the PV modules assumed to be in open circuit mode. Thermal and electrical efficiencies of the CPVT collector are plotted as a function of ($T_{m,f}$-T_{amb}) in Fig. 18.

It is observed that the slope of the thermal efficiency curve is steeper than the electrical efficiency curve. So, the temperature difference ($T_{m,f}$-T_{amb}) variations have a significant effect on the thermal efficiency, and the electrical efficiency has a much lower dependency on the temperature difference. The thermal collector efficiency is dependent on (T_{mf}-T_{amb}), while the solar cell efficiency is dependent on T_{PV}. However, $T_{m,f}$ affects T_{pv}, depending on the thermal resistance between them. The temperature difference between PV cells and the HTF mean temperature (T_{PV}-T_{mf}) is decreasing with increasing (T_{mf}-T_{amb}). If the collector is not cooled and reaches stagnation temperature T_{PV} = T_{mf}. It is found that by a 50 °C increase in the temperature difference ($T_{m,f}$-T_{amb}), the

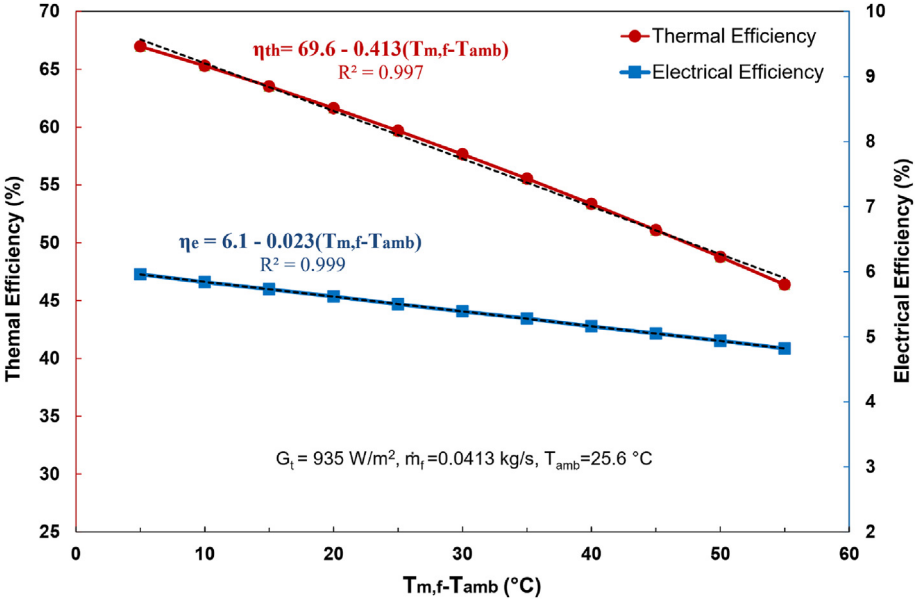

Fig. 18. Thermal and Electrical efficiencies as a function of ($T_{m,f}$-T_{amb}).

thermal and electrical efficiencies were decreased by 31% and 19%, respectively.

By considering a linear temperature dependence of the thermal efficiency (Fig. 18), the characteristic equation of the CPVT collector thermal efficiency can be determined as follows (Eq. (54)):

$$\eta_{th} = 69.6 + 386.2\left(\frac{T_{m,f} - T_{amb}}{G_t}\right) \quad (54)$$

Which is derived by multiplying the second term of the thermal efficiency equation (given in Fig. 18) by 935 W/m^2.

6. Conclusions

The main objective of the present study is to develop a 0-D thermal model to evaluate the performance of a novel CPVT collector for the first time. Also, an experimental test of the collector was performed for two days (July 27 and August 27) with different operating conditions and the thermal model was validated by the experimental results with a reasonable deviation. So, it is concluded that the model works properly and gives realistic results. The trend of the model results follows the trend of solar radiation flux and solar angles.

It is found that by removing the glass cover, the optical losses reduce but the thermal losses increase and so the thermal output significantly decreases. The daily average (from 9:00 to 15:00) thermal power output of the CPVT collector is reduced by 13% and the daily average electrical power output increases by 10%. It is observed that by removing the glass cover in the developed model during August 27, the daily average equivalent primary energy of the collector decreases by 9%. So, although removing the glass cover is good for electricity yield, it is not desirable from overall primary energy perspective.

The effect of HTF inlet temperature variation on the thermal and electrical yield of the collector was studied. It is understood that by increasing the HTF inlet temperature from 15 to 65 °C, the calculated thermal and electrical outputs at noon of August 27 decrease by 26% and 18%, respectively. So, the thermal power sensitivity to HTF inlet temperature is higher than electrical power sensitivity.

Also, the effect of the HTF mass flow rate on the collector outputs was investigated. By changing the HTF mass flow rate from 0.005 kg/s to 0.015 kg/s, the transition of laminar to turbulent flow occurs and so a sharp change in the thermal and electrical power was observed. Therefore, it is recommended to use HTF flow rates higher than 0.015 kg/s for a better performance of the collector. By increasing the HTF mass flow rate, pump electricity consumption and thermal and electrical power output of the CPVT collector increase. Conversely, the HTF outlet temperature that indicates the quality of the thermal energy is decreased. In practice, it should be noted that heat with low temperature (quality) cannot be used directly in the solar heating system and it needs an auxiliary heater. It is understood that by increasing mass flow rate, the net electrical power output of the collector first rises to a maximum (0.045 kg/s) and then drops because of a higher rate of pump consumption decrease than electricity generation increase. For higher than 0.045 kg/s mass flow rates, although the net electricity generation decrease, the thermal power output still increases. It is observed that the primary energy saving reaches a maximum amount of 954.5 W/m^2 at 0.095 kg/s and then decreases. The optimum mass flow rates for net electricity yield and primary energy saving under the mentioned operating conditions of the collector were found to be 0.045 kg/s and 0.95 kg/s, respectively.

The effect of the temperature difference between mean fluid temperature and ambient temperature ($T_{m,f}$-T_{amb}) on the thermal and electrical efficiencies was studied. It is understood that by increasing ($T_{m,f}$-T_{amb}) from 5 °C to 55 °C, the thermal and electrical power decreases by 31% and 19%, respectively, which leads to a sharper slope of thermal efficiency changes. The maximum thermal and electrical efficiencies of the collector for the investigated conditions were found to be 69.6% and 6.1%, respectively. The characteristic equation of the CPVT collector thermal efficiency was obtained.

CRediT authorship contribution statement

Hossein Afzali Gorouh: Methodology, Conceptualization, Software, Validation, Writing – original draft, Visualization, Formal analysis, Investigation. **Mazyar Salmanzadeh:** Supervision, Conceptualization, Methodology, Writing – review & editing, Project administration. **Pouriya Nasseriyan:** Software, Validation, Writing – review & editing, Data curation. **Abolfazl Hayati:** Project administration, Funding acquisition, Conceptualization, Writing – review & editing, Supervision, Resources. **Diogo Cabral:** Investigation, Validation, Data curation, Writing – review & editing, Resources. **João Gomes:** Resources, Investigation, Data curation, Conceptualization, Writing – review & editing. **Björn Karlsson:** Supervision, Conceptualization, Methodology, Writing – review & editing.

Declaration of competing interest

The authors declare that they have no known competing financial interests or personal relationships that could have appeared to influence the work reported in this paper.

Acknowledgments

This study was partly funded by the Swedish Foundation for International Cooperation in Research and Higher Education (Grant No. ME2018-7559). The authors gratefully acknowledge the fruitful collaboration and support provided by the University of Gävle and Mr. Sadegh Sajedi for design and build of the collector. The authors are thankful for the assistance and support provided by the office of international relations and vice-chancellor of research and technology of the Shahid Bahonar University of Kerman. The authors would like to extend their sincere appreciation to Prof. Mehran Ameri and Prof. Seyed Hossein Mansouri for their kind assistance and continuous guidance.

References

[1] P.G. Charalambous, G.G. Maidment, S.A. Kalogirou, K. Yiakoumetti, Photovoltaic thermal (PV/T) collectors: a review, Appl. Therm. Eng. 27 (2007) 275–286, https://doi.org/10.1016/j.applthermaleng.2006.06.007.

[2] G.N. Tiwari, R.K. Mishra, S.C. Solanki, Photovoltaic modules and their applications: a review on thermal modelling, Appl. Energy 88 (2011) 2287–2304, https://doi.org/10.1016/j.apenergy.2011.01.005.

[3] R. McConnell, A solar concentrator pathway to low-cost electrolytic hydrogen, in: K. Rajeshwar, R. McConnell, S. Licht (Eds.), Sol. Hydrog. Gener. Towar. A Renew. Energy Futur., Springer New York, New York, NY, 2008, pp. 65–86, https://doi.org/10.1007/978-0-387-72810-0_4.

[4] H.P. Garg, R.S. Adhikari, Performance analysis of a hybrid photovoltaic/thermal (PV/T) collector with integrated CPC troughs, Int. J. Energy Res. 23 (1999) 1295–1304, https://doi.org/10.1002/(SICI)1099-114X(199912)23:15<1295::AID-ER553>3.0.CO;2-T.

[5] J.S. Coventry, Performance of a concentrating photovoltaic/thermal solar collector, in: Sol. Energy, Pergamon, 2005, pp. 211–222, https://doi.org/10.1016/j.solener.2004.03.014.

[6] J. Nilsson, H. Håkansson, B. Karlsson, Electrical and thermal characterization of a PV-CPC hybrid, Sol. Energy 81 (2007) 917–928, https://doi.org/10.1016/j.solener.2006.11.005.

[7] L.R. Bernardo, B. Perers, H. Håkansson, B. Karlsson, Performance evaluation of low concentrating photovoltaic/thermal systems: a case study from Sweden, Sol. Energy 85 (2011) 1499–1510, https://doi.org/10.1016/j.solener.2011.04.006.

[8] F. Calise, A. Palombo, L. Vanoli, A finite-volume model of a parabolic trough photovoltaic/thermal collector: energetic and exergetic analyses, Energy 46 (2012) 283–294, https://doi.org/10.1016/j.energy.2012.08.021.
[9] H.M. Bahaidarah, B. Tanweer, P. Gandhidasan, N. Ibrahim, S. Rehman, Experimental and numerical study on non-concentrating and symmetric unglazed compound parabolic photovoltaic concentration systems, Appl. Energy 136 (2014) 527–536, https://doi.org/10.1016/j.apenergy.2014.09.060.
[10] D. Atheaya, A. Tiwari, G.N. Tiwari, I.M. Al-Helal, Analytical characteristic equation for partially covered photovoltaic thermal (PVT) compound parabolic concentrator (CPC), Sol. Energy 111 (2015) 176–185, https://doi.org/10.1016/j.solener.2014.10.025.
[11] R. Tripathi, G.N. Tiwari, I.M. Al-Helal, Thermal modelling of N partially covered photovoltaic thermal (PVT) - compound parabolic concentrator (CPC) collectors connected in series, Sol. Energy 123 (2016) 174–184, https://doi.org/10.1016/j.solener.2015.11.014.
[12] G.N. Tiwari, M. Meraj, M.E. Khan, R.K. Mishra, V. Garg, Improved Hottel-Whillier-Bliss equation for N-photovoltaic thermal-compound parabolic concentrator (N-PVT-CPC) collector, Sol. Energy 166 (2018) 203–212, https://doi.org/10.1016/j.solener.2018.02.058.
[13] I.P. Koronaki, M.T. Nitsas, Experimental and theoretical performance investigation of asymmetric photovoltaic/thermal hybrid solar collectors connected in series, Renew. Energy 118 (2018) 654–672, https://doi.org/10.1016/j.renene.2017.11.049.
[14] D. Cabral, B.O. Karlsson, Electrical and thermal performance evaluation of symmetric truncated C-PVT trough solar collectors with vertical bifacial receivers, Sol. Energy 174 (2018) 683–690, https://doi.org/10.1016/j.solener.2018.09.045.
[15] T. Maatallah, W. Ben Youssef, Simulation and performance analysis of concentrating photovoltaic/thermal collector (CPV/T) with three-sided thermal insulation based on coupled optothermal model, Sol. Energy 181 (2019) 308–324, https://doi.org/10.1016/j.solener.2019.02.002.
[16] H. Zhang, K. Liang, H. Chen, D. Gao, X. Guo, Thermal and electrical performance of low-concentrating PV/T and flat-plate PV/T systems: a comparative study, Energy 177 (2019) 66–76, https://doi.org/10.1016/j.energy.2019.04.056.
[17] P. Nasseriyan, H. Afzali Gorouh, J. Gomes, D. Cabral, M. Salmanzadeh, T. Lehmann, A. Hayati, Numerical and experimental study of an asymmetric CPC-PVT solar collector, Energies 13 (2020) 1669, https://doi.org/10.3390/en13071669.
[18] M. Blanco, A. Mutuberria, D. Martinez, Experimental validation of Tonatiuh using the Plataforma Solar de Almería secondary concentrator test campaign data, Proc. SolarPACES (2010).
[19] M. Blanco, A. Mutuberria, A. Monreal, R. Albert, Results of the empirical validation of Tonatiuh at Mini-Pegase CNRS-PROMES facility, in: Proc. 17th SolarPACES Int. Symp. Conc. Sol. Power, Chem. Energy, 2011.
[20] T.L. Bergman, F.P. Incropera, D.P. DeWitt, A.S. Lavine, Fundamentals of Heat and Mass Transfer, John Wiley & Sons, 2011.
[21] J.R. Howell, R. Siegel, Thermal Radiation Heat Transfer, CRC Press, 2010.
[22] S.A. Kalogirou, Solar Energy Engineering: Processes and Systems, Academic Press, 2013.
[23] M. Al-Arabi, B. Sakr, Natural convection heat transfer from inclined isothermal plates, Int. J. Heat Mass Tran. 31 (1988) 559–566, https://doi.org/10.1016/0017-9310(88)90037-3.
[24] D.L. Evans, Simplified method for predicting photovoltaic array output, Sol. Energy 27 (1981) 555–560, https://doi.org/10.1016/0038-092X(81)90051-7.
[25] B.R. Rich, An investigation of heat transfer from an inclined flat plate in free convection, Trans. ASME. 75 (1953) 489–499.
[26] S.W. Churchill, H.H.S. Chu, Correlating equations for laminar and turbulent free convection from a vertical plate, Int. J. Heat Mass Tran. 18 (1975) 1323–1329, https://doi.org/10.1016/0017-9310(75)90243-4.
[27] F. Kreith, R.M. Manglik, M.S. Bohn, in: Principles of Heat Transfer, SI Edition, Cengage Learning, 2012.
[28] V. Gnielinski, New equations for heat and mass transfer in turbulent pipe and channel flow, Int. Chem. Eng. 16 (1976) 359–368.
[29] S.M. Elsherbiny, Free convection in inclined air layers heated from above, Int. J. Heat Mass Tran. 39 (1996) 3925–3930, https://doi.org/10.1016/0017-9310(96)00047-6.
[30] Y.A. Çengel, J.M. Cimbala, R.H. Turner, Fundamentals of Thermal-Fluid Sciences, McGraw-Hill Education, 2012.
[31] United Nations, Glossary of Environment Statistics, Studies in Methods, United Nations publication, New York, 1997.
[32] ISO 52000-1, Energy Performance of Buildings - Overarching EPB Assessment - Part 1: General Framework and Procedures, International Organisation for Standardisation, 2017.
[33] ISO 9806, ISO 9806:2013 Solar energy - solar thermal collectors - test methods, 2013.